Formation of antihydrogen in three-body antiproton-positron collisions

S. Roy, S. Ghosh Deb, and C. Sinha
Theoretical Physics Department, Indian Association for the Cultivation of Science, Kolkata-700032, India
(Received 19 March 2008; published 8 August 2008)

A quantum-mechanical approach is proposed for the formation of antihydrogen ($\bar{H}$) in the ground and excited states ($2s,2p$) via the mechanism of three-body recombination (TBR) inside a trapped plasma of antiprotons ($\bar{p}$) and positrons (e^+) or in the collision between the two beams of them. Variations of the differential as well as the total formation cross sections are studied as a function of the incident energies of both the active and the spectator e^+'s. Significantly large cross sections are found at very low incident energies in the TBR process as compared to other processes leading to antihydrogen. The present ($\bar{H}$) formation cross section decreases with increasing positron energy (temperature) but no simple power law could be predicted for it covering the entire energy range ($\sim$5–50 eV), corroborating the experimental findings qualitatively, the latter being at a much lower energy regime ($\sim 10^{-4}$ eV). The formation cross sections are found to be much higher for unequal energies of the two e^+'s than for equal energies, as expected physically.

DOI: 10.1103/PhysRevA.78.022706 PACS number(s): 34.80.Lx, 36.10.−k

I. INTRODUCTION

Production of antihydrogen, the simplest and most stable bound state of antimatter is one of the current topics both from the experimental and the theoretical perspectives mainly because its study provides various fundamental differences between matter and antimatter. Particularly, the cold antihydrogen ($\bar{H}$) atom is an ideal system for studying the fundamental symmetries in physics, e.g., the CPT invariance theorem in the standard quantum field theory and the gravitational weak equivalence principle for antimatter. The major challenge facing the $\bar{H}$ research is the production of cold and trapped ground state $\bar{H}$ that is needed for the precise laser spectroscopy. Apart from these, there are many important practical applications of the $\bar{H}$ out of which the followings are worthy to be mentioned. First, the antihydrogen may also be used for igniting inertial confinement fusion pellets, the feasibility of which was already investigated [1]. Second, the antihydrogen finds important applications in the propulsion system [2].

In view of the recent technological advances in the cooling and trapping mechanism of antiprotons ($\bar{p}$) and positrons (e^+), the long term goal for the production of cold and trapped $\bar{H}$, necessary for the high precision spectroscopic studies has now become possible. This has motivated theoretical workers to venture different processes producing antihydrogen. The most important of these processes is the following three-body recombination (TBR): $\bar{p}+e^++e^+ \rightarrow \bar{H}+e^+$ (process I) in which a spectator particle carries away the excess energy and the momentum released in the recombination. The above reaction poses to be more efficient by orders of magnitude [3–5] compared to other $\bar{H}$ production processes, e.g., the radiative recombination (RR) [6–8], the three-body charge transfer between the Ps and the $\bar{p}$ [9–20] at low incident energies. The main reason for this is due to the following. The spectator positron in the TBR process efficiently carries off the extra energy, unlike the other $\bar{H}$ production reactions. Another important advantage of the process I is that the reactants are stable charged particles which can be held in a trap for cooling and then subsequently for the recombination to occur. In fact, it is found experimentally [3–5] that the TBR in the trapped plasma of antiproton and positrons happens to be the most efficient $\bar{H}$ production reaction at very low incident energies. However, the main disadvantage of the TBR is that the $\bar{H}$ is favorably formed in the excited states [3], although for the high precision spectroscopic studies, the ground state $\bar{H}$ is much needed. In contrast, in the RR process, although the ground state is favored, the cross section itself is much lower [3–5] particularly at very low-incident energies. In fact at the experimental extreme low-energy regime ($\sim 10^{-4}$ eV), the RR has no contribution while at the present energy range (5–50 eV) the RR has significant contributions [7], although much smaller than the TBR. However, at still higher energies (e.g., 100 eV), the RR process [7] is found to overtake the TBR (see Table I).

Regarding the experimental situation for the TBR process, the three main international groups are working on it at CERN, i.e., the ATHENA [21–26] and ATRAP collaborations [27–31] and the group located at Harvard University [32–34] while another group from Riken [35,36] is also concentrating on the experiments of cold and trapped $\bar{H}$ production. In all the experiments attention is being paid mainly to the temperature dependence of the $\bar{H}$ production at extreme low energies. In fact, all the TBR experiments are limited to incident energies in the range of meV ($\sim 3.5 \times 10^{-4}$ eV). Further, a strong magnetic field ($\sim$5.4 T) is applied which is necessary for the confinement of the reaction constituents inside the trap.

The present study which addresses the same TBR process for the production of $\bar{H}$, corresponds to somewhat different experimental situations (to be described later) and the model has the following limitations and assumptions in the context of the existing experiments [21–36].

(1) The energy range considered in the present work is relatively much higher ($\sim$5–50 eV) as compared to the experiment (meV range).

(2) No effect of the external magnetic field is incorporated in the present model.

(3) The heavy antiproton is treated as a stationary target while in the experiment the antiprotons are injected through the positron cloud so their velocities are comparable.

The present model corresponds to the following situations. We consider an ensemble of weakly correlated positrons and the e^+ plasma density is assumed to be low enough so that the e^+-e^+ interaction can be treated as a perturbation. Since the recombination reaction requires a third body for the energy and momentum conservation of the process, another e^+ of the plasma serves this purpose and the process becomes a TBR one. The antiproton is treated as a stationary ionic target located at the origin of coordinates which corresponds to the experimental situation of a cold and trapped $\bar{p}$. In other words, the antiproton is treated as infinite mass. However, this approximation (done for convenience of calculations) seems to be reasonable since the mass of the antiproton is about 1840 times the mass of e^+ [37]. Further, this approximation makes sense when the e^+ motion is rapid compared to the ion motion [37,38]. In fact, the stationary target corresponds to the laboratory frame which we found to be more convenient than the center of mass frame for the present theoretical treatment of the TBR reaction. It may be mentioned in this context that the total cross section for the process is the same for both laboratory and center of mass systems, although there is a change in the differential cross sections [39].

There is also a probability of exchange between the active and the spectator positrons which is also incorporated in the present prescription in a proper way. However, in the recent experimental context where the $\bar{p}$'s are injected through the e^+ cloud, the above assumption (stationary $\bar{p}$) is not well justified as the $\bar{p}$ and the e^+ move with comparable velocities. Further, the neglect of an external magnetic field in the present model might also have some effects on the present results [5,37,38].

As for the theoretical situation for the $\bar{H}$ production through TBR, the first detailed study is due to Robicheaux [37] in the framework of classical trajectory Monte Carlo (CTMC) method. However, in this calculation the Author introduced some fraction of electrons along with the e^+ as well as a strong magnetic field in order to make the process feasible. It was noted [37] that the $\bar{H}$ formation reduces substantially in presence of the e^-'s. Prior to and also following this work [37], there exist some calculations by the same author [40,41] that mainly study the temperature dependence of the TBR process based on some statistical models.

The present study deals with the differential and the total $\bar{H}$ formation cross sections in ground and excited $(2s,2p)$ states through the TBR mechanism in the collision between the positron and the $\bar{p}$ plasma at much higher incident energies as compared to the existing low-energy experiments. Although experimentally the TBR process favors the $\bar{H}$ formation in highly excited states, for the theoreticians it is much easier to calculate the cross sections in the ground and low lying states. Thus in the absence of any experimental cross section data, the present theoretical estimates of the ground and excited $(2s,2p)$ states $\bar{H}$ formation cross sections might give some stimulus and guidelines to the future detailed experiments.

II. THEORY

The present study deals with the following three-body recombination process:

$$\bar{p} + e^+ + e^+ \rightarrow \bar{H} + e^+. \tag{1}$$

The prior form of the transition amplitude T_{if} for this process is given by

$$T_{if} = \langle \Psi_f^-(\vec{r}_1,\vec{r}_2)(1+\mathbf{P})|V_i|\psi_i(\vec{r}_1,\vec{r}_2)\rangle, \tag{2}$$

where $\mathbf{P}$ denotes the exchange operator corresponding to the interchange of the positrons in the final channel. V_i in Eq. (2) is the initial channel perturbation which is the part of the total interaction not diagonalized in the initial state and ψ_i is the corresponding asymptotic wave function. The final channel wave function Ψ_f^- satisfies the three-body Schrödinger equation obeying the incoming wave boundary condition

$$(H-E)\Psi_f^- = 0. \tag{3}$$

The total Hamiltonian (H) of the system can be written as

$$H = -\frac{1}{2}\nabla_1^2 - \frac{1}{2}\nabla_2^2 - \frac{1}{r_1} - \frac{1}{r_2} + \frac{1}{r_{12}}, \tag{4}$$

where $\vec{r}_1$ and $\vec{r}_2$ represent the position vectors of the active e^+ (to be transferred) and the spectator e^+'s, respectively. The atomic unit (a.u.) is used throughout the work.

The initial channel asymptotic wave function ψ_i in Eq. (2) satisfies the following Schrödinger equation:

$$\left(-\frac{1}{2}\nabla_1^2 - \frac{1}{2}\nabla_2^2 - \frac{1}{r_1} - \frac{1}{r_2} - E\right)\psi_i = 0 \tag{5}$$

and is given by

$$\psi_i = N_j e^{i\vec{k}_j\cdot\vec{r}_j} {}_1F_1[i\alpha_j, 1, -i(k_j r_j - \vec{k}_j\cdot\vec{r}_j)], \tag{6}$$

with $N_j = \exp(\frac{-\pi\alpha_j}{2})\Gamma(1-i\alpha_j)$, $j=1,2$, $\alpha_j = -\frac{1}{k_j}$, and $\vec{k}_j$ denotes the incident momentum of the active or the spectator e^+, respectively. The approximated final state wave function Ψ_f^- is chosen in the framework of the Eikonal approximation as follows:

$$\Psi_f^- = \phi_f(r_1) e^{i\vec{k}_f\cdot\vec{r}_2} \exp\left[i\eta_f \int_z^\infty \left(\frac{1}{r_{12}} - \frac{1}{r_2}\right) dz' \right] \tag{7}$$

with $\eta_f = \frac{1}{k_f}$, k_f being the final momentum of the spectator e^+;

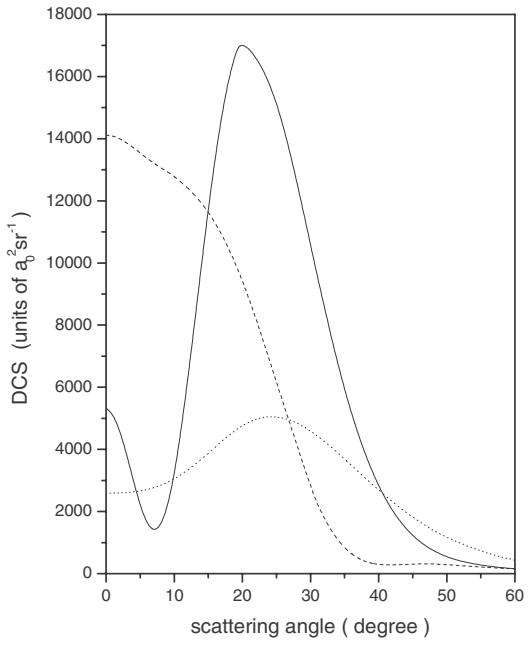

FIG. 1. Differential cross sections (DCSs) (in a_0^2 sr^{-1}) for antihydrogen formation in 1s, 2s, and 2p states in antiproton-positron -positron collisions for incident energy $E_1=E_2=10$ eV. The solid line is for 2p, dashed line for 2s, and dotted line for 1s states. 1s results are scaled up by 2.5 times.

$\phi_f(r_1)$ represents the bound state wave function of the $\bar{H}$ atom.

Finally the differential cross section for the process (1) is given by

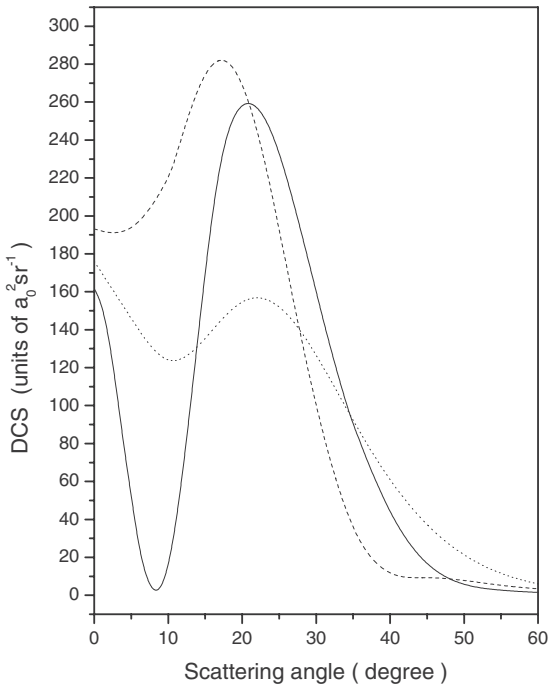

FIG. 2. Same DCS as in Fig. 1 but for $E_1=E_2=20$ eV. The solid line is for 2p, dashed line for 2s, and dotted line for 1s states.

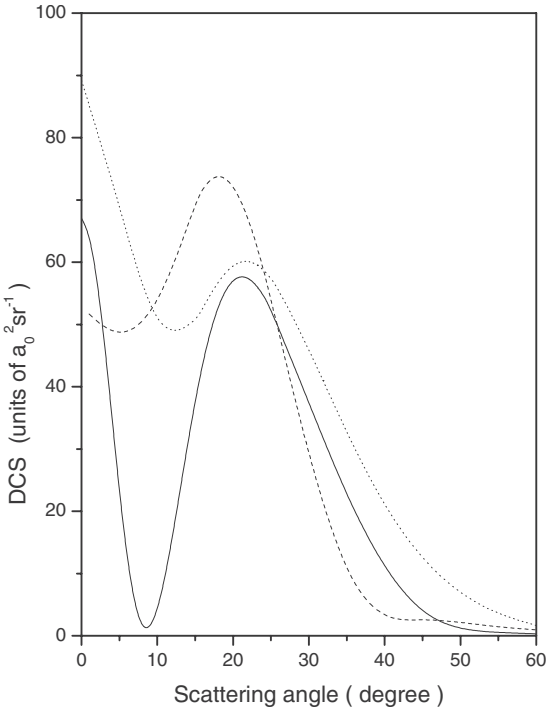

FIG. 3. Same DCS as in Fig. 1 but for $E_1=E_2=25$ eV. The solid line is for 2p, dashed line for 2s, and dotted line for 1s states.

$$\frac{d\sigma}{d\Omega} = \frac{k_f}{k_1 k_2}\left[\frac{1}{4}(|f+g|^2) + \frac{3}{4}(|f-g|^2)\right], \tag{8}$$

where f and g corresponds to the direct and the exchange amplitudes, respectively.

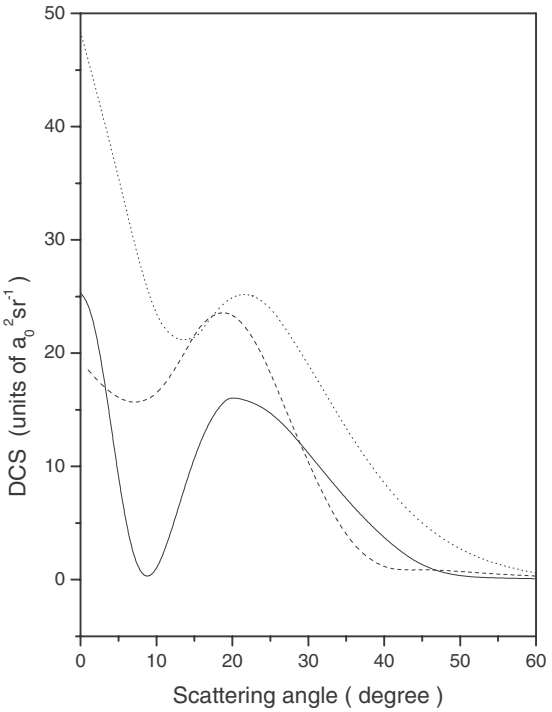

FIG. 4. Same DCS as in Fig. 1 but for $E_1=E_2=30$ eV. The solid line is for 2p, dashed line for 2s and dotted line for 1s states.

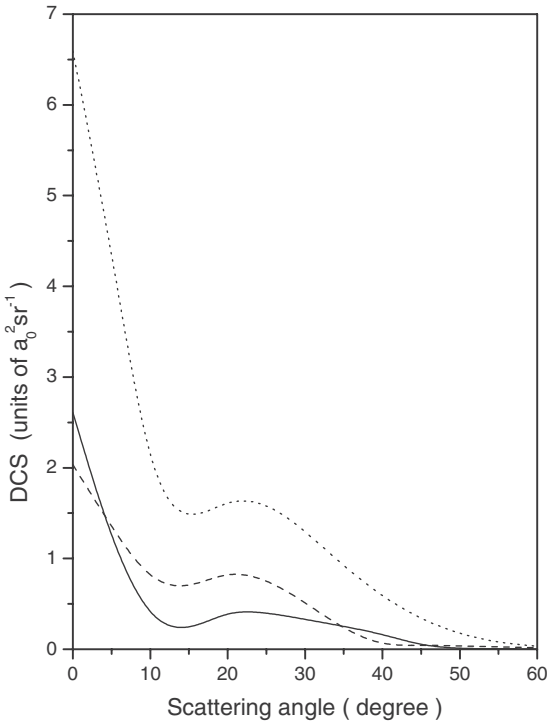

FIG. 5. Same DCS as in Fig. 1 but for $E_1=E_2=50$ eV. The solid line is for $2p$, dashed line for $2s$, and dotted line for $1s$ states.

Using the following contour integral representations of the Eikonal phase factors [42] as well as the Coulomb functions [43] and after much analytical reductions [44,45], the transition matrix element (2) is finally reduced [46,47] to a three-dimensional integral which is evaluated numerically by using different quadrature methods. The Eikonal phase factor is of the form

$$y^{\pm(i\eta-n)} = \frac{(-1)^{n+1}}{2i\sin(\mp\pi i\eta)\Gamma(\mp i\eta \pm n)} \times \int_c (-\lambda)^{\mp i\eta \pm n-1} \exp(-\lambda y)dy, \tag{9a}$$

where the contour c has a branch cut from 0 to ∞ [42]; the confluent hypergeometric function

$${}_1F_1(i\alpha,1,z) = \frac{1}{2\pi i}\int_{\Gamma_1}^{(0^+,1^+)} p(\alpha,t)\exp(zt)dt \tag{9b}$$

with $p(\alpha,t)=t^{-1+i\alpha}(t-1)^{-i\alpha}$, Γ_1 is a closed contour encircling the two points 0 and 1 once anticlockwise [43]. At the point where the contour crosses the real axis to the right side of 1, arg$t$ and arg$(t-1)$ are both zero.

III. RESULTS AND DISCUSSIONS

We have computed the $\bar{H}$ formation cross sections both differential and total for the TBR process (1) in the framework of the Coulomb distorted Eikonal approximation (CDEA), where distortions have been included in both the channels. The exchange between the active and the spectator e^+'s is also incorporated. Since the present process (1) is an exothermic reaction it can occur even at zero incident energy. However, our results are not converged below 5 eV due to computational problems and are therefore not reported here. Furthermore, it may be mentioned that the present model might not yield very reliable results at extreme low energies where the recent experiments are mainly concentrating upon.

Figures 1–5 exhibit the present differential cross sections (DCSs) in the ground and excited states ($2s$ and $2p$) for different incident energies of both the positrons, e.g., $E_1=E_2=10$, 20, 25, 30, and 50 eV, respectively. The figures

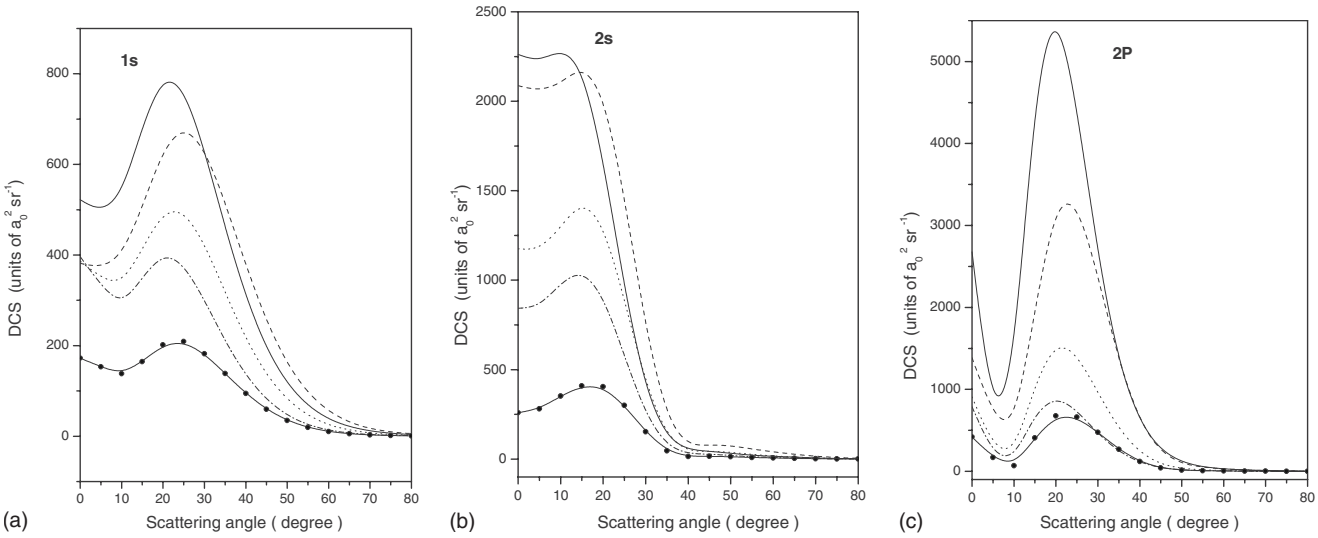

FIG. 6. (a) Differential cross sections (in a_0^2 sr^{-1}) for antihydrogen formation in the $1s$ state in antiproton-positron-positron collisions for different values of E_1 and E_2. The solid line is for $E_1=15$, $E_2=10$ eV, dashed line for $E_1=10$, $E_2=15$ eV, dotted line for $E_1=15$, $E_2=15$ eV, dashed dot line for $E_1=20$, $E_2=15$ eV, solid line with circles for $E_1=15$, $E_2=20$ eV. (b) Same as (a) but for $\bar{H}$ formation in the $2s$ state. (c) Same as (a) but for $\bar{H}$ formation in the $2p$ state.

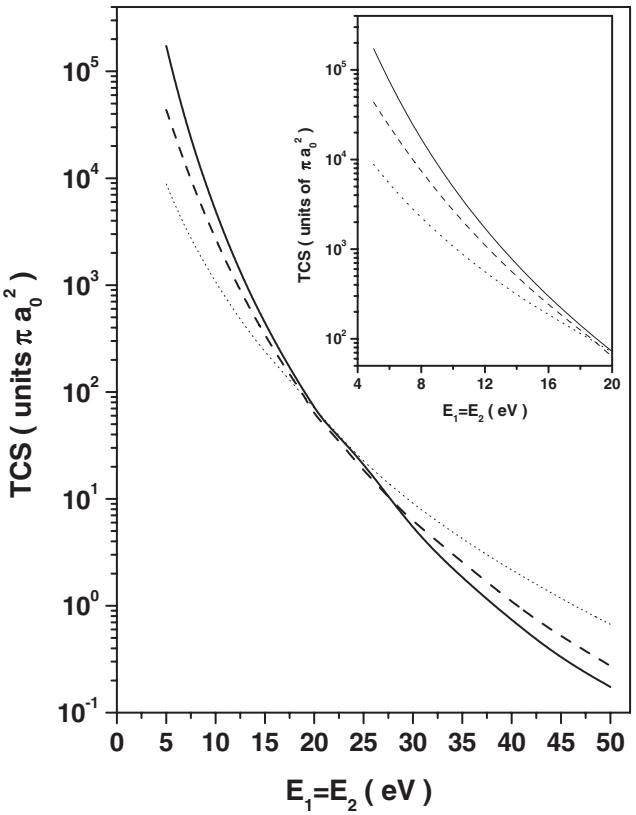

FIG. 7. Partial total cross sections (TCSs) (units of πa_0^2) for antihydrogen formation in $1s$, $2s$, $2p$ states for the wider range of incident energy (0–50 eV) where $E_1=E_2$. The solid line is for $2p$ state, dashed line for $2s$ state, dotted line for $1s$ states. Inset: same TCS but for small range of incident energy.

reveal that the $\bar{H}$ formation (in all the states) is strongly favored in the forward directions and as such the DCS are presented up to 60° only, beyond which the cross sections become negligible. At very low incident energy, the magnitude of the formation cross section is found to be largest for the $2p$ state and smallest for the $1s$ state while the $2s$ lies in between, i.e., $2p>2s>1s$ (see Fig. 1). This trend of the DCS is noted up to 15 eV (not shown in the figure), although with increasing incident energy, the maximum of the $2p$ DCS decreases and tends towards the $2s$ maximum so that at $E_1=E_2=20$ eV, the $2s$ overtakes the $2p$ (see Fig. 2). The DCS peak in this case is in the order $2s>2p>1s$. In contrast, at intermediate and high incident energies (~25 eV onwards), the DCS is maximum for the $1s$ state and minimum for the $2p$ state while the $2s$ lies in between (i.e., $1s>2s>2p$, Figs. 3–5).

As for the position of the DCS maximum, at low incident energies (~ up to 15 eV), the $1s$ and $2p$ maxima lie at some lower scattering angles (~20°) while the $2s$ maximum occurs at the extreme forward (~0°). With increasing energy, the DCS maxima for these two states ($1s$ and $2p$) move towards the extreme forward (~0°), while the $2s$ maximum moves in the reverse direction (see Figs. 2–4). However, at high incident energies (e.g., ~40 eV onwards), all the partial DCS maxima are finally peaked at extreme forward 0° (see Fig. 5), as expected.

Figures 6(a)–6(c) again exhibit the partial DCS but for some unequal energies of the two incident e^+'s (i.e., $E_1\neq E_2$) along with a case for $E_1=E_2$ (15 eV) for the sake of comparison. The following interesting features are noted from the figures. All the partial DCS are found to be much higher (by a factor of ~2 to 2.5) when the energy of the active e^+ (E_1) is greater than that of the spectator one (E_2), i.e., when $E_1>E_2$. The DCS for unequal ($E_1\neq E_2$) energies

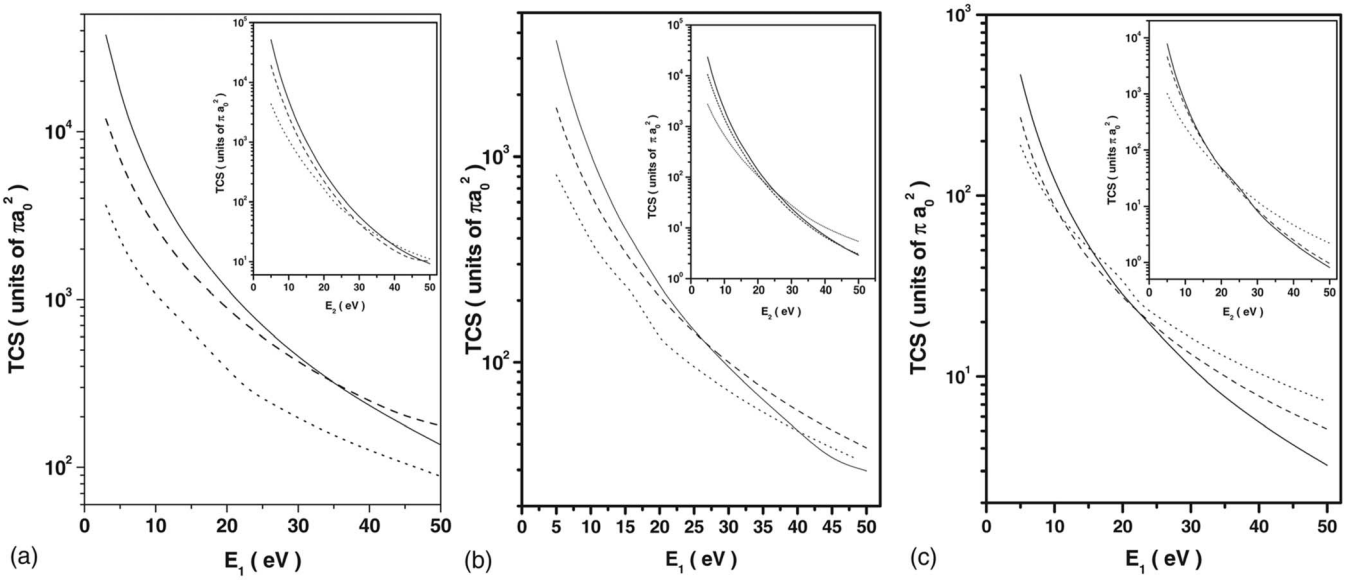

FIG. 8. (a) Partial total cross sections (units of πa_0^2) for antihydrogen formation in $1s$, $2s$, $2p$ states with respect to E_1 for $E_2=10$ eV. Inset: same TCS but with respect to E_2 for $E_1=10$ eV. Solid line for the $2p$ state, dashed line for $2s$ state, dotted line for $1s$ state. (b) Same as (a) but for $E_2=15$ eV. Inset: same as the inset of (a) but for $E_1=15$ eV. (c) Same as (a) but for $E_2=25$ eV. Inset: same as the inset of (a) but for $E_1=25$ eV.

TABLE I. Present TCS for $\bar{H}$ formation in the ground $(1s)$ and excited $(2s,2p)$ states along with different theoretical [7,15,18,20] results.

Energy (eV)	RR [7] process	Mitroy *et al.* [15]		Mitroy *et al.* [18]			Sinha *et al.* [20]		Present results		
		$1s$	$(2s+2p)$	$1s$	$2s$	$2p$	FF$(1s)$	FA$(1s)$	$1s$	$2s$	$2p$
10.0	0.880						1.37	12.18	1074	2705	4923
13.60		1.923	8.440	1.460	0.660	3.810	0.920	8.320	373.07	705.4	530.06
20.40				0.940	0.254	1.760	0.470	3.990	68.25	59.62	36.13
25.84		0.735	1.729				0.290	2.050	23.16	15.43	11.048
34.00				0.394	0.080	0.396	0.160	0.650	5.14	3.29	1.21
43.52		0.240	0.280				0.080	0.19	1.38	0.73	0.21
54.40				0.130	0.030	0.060	0.040	0.090	0.51	0.21	0.65
63.92		0.078	0.053				0.020	0.050	0.16	0.06	0.03
100.0	0.025						0.005	0.007	0.0134	0.0048	0.0035

lie much above than those for equal energies $(E_1=E_2)$. This is quite expected physically due to strong repulsion between the two e^+ s at equal energies.

Next we come over to the total cross sections (TCSs) for the $\bar{H}$ formation displayed in Figs. 7 and 8 for different sets of incident energies. Figure 7 displays the partial TCS when the two incident e^+'s share equal energy $(E_1=E_2)$. As in the case of DCS, at low and intermediate incident energies ($\sim$ up to 20 eV), the partial TCS follows the order $2p>2s>1s$ (inset of Fig. 7), while beyond 25 eV it is in the decreasing order with excitation of the $\bar{H}$ state, i.e., $1s>2s>2p$. The dominance of the $2p$ TCS at low incident energies could probably be attributed to the long range polarization effects which is much stronger for the $2p$ state than for any other states. In fact, a major contribution to the polarization effect that mainly dominates at lower incident energies, comes from the lowest lying p state (i.e., $2p$ state). Figure 7 also indicates that although all the partial TCS decrease monotonically with increasing incident energy, they do not follow any simple power law, corroborating the experimental findings [22,24].

Figures 8(a)–8(c) display the partial TCS against the active e^+ energy (E_1) for some fixed values of E_2 (spectator) while the insets exhibit the reverse, i.e., TCS vs E_2 for fixed E_1. As in the case of DCS, for a fixed sum of E_1 and E_2, the partial TCS is found to be larger when $E_1>E_2$ than for $E_1<E_2$. Further, the TCS against E_2 falls off much more rapidly than the TCS versus E_1 (see Figs. 8 and their insets). Regarding the relative magnitude of the partial TCS, for the lower energy of the spectator e^+, e.g., $E_2=10$ eV [Fig. 8(a)], the general trend of the TCS follows the order $2p>2s>1s$ at low and intermediate E_1 while at higher E_1, the above order changes to $2s>2p>1s$. A similar behavior is noted in Fig. 8(b) (for $E_2=15$ eV) as in Fig. 8(a) with some exceptions at higher E_1. At intermediate E_2 [25 eV, Fig. 8(c)], the partial TCS follow different orders for different ranges of E_1, e.g., at lower E_1 the $2p$ dominates while at higher E_1 the $1s$ dominates. However, at higher E_2 $(\sim E_2 \geqslant 50$ eV), the $1s$ cross section dominates through out the range of E_1 except at very low energies $(E_1 \sim 5-10$ eV) where the $2s$ is most prominent (not shown in figure).

For the sake of some numerical measures, we have displayed in Table I the present partial $(1s,2s,2p)$ TCS along with some other existing theoretical results due to Mitroy *et al.* [15,18] for the process $\bar{p}+Ps \rightarrow \bar{H}(n,l,m)+e^+$ using unitarized Born approximation [18] and close coupling approximation [15]. Results due to Sinha *et al.* [20] for the above process in the Eikonal approximation both with and without laser field and results due to Li *et al.* [7] for the e^+-$\bar{p}$ RR process are also included in Table I. The incident energies are chosen in accordance with their [7,15,18] calculations. The field assisted (FA) results [20] are presented for the field strength 0.01 a.u. and the frequency 0.043 a.u.

Table I reveals that the present TBR cross sections are much larger than all the other processes leading to antihydrogen throughout the energy range considered, except at very high energy (e.g., 100 eV), where the RR process [7] dominates the TBR. It may be mentioned in this context that the RR process was found to be unimportant for high e^+ density and low temperature [5,37].

Table II displays the probable power laws obeyed by the partial as well as the sum TCS for different incident energy ranges of the e^+ corresponding to Figs. 7 $(E_1=E_2)$ and 8 $(E_1 \neq E_2)$.

TABLE II. Power laws obeyed by the partial as well as the sum TCS for different incident energy ranges.

Energy range (in eV)	Power law obeyed			
$E_1=E_2$	$1s$	$2s$	$2p$	$1s+2s+2p$
5–10	$\sim E^{-2.9}$	$\sim E^{-3.7}$	$\sim E^{-4.8}$	$\sim E^{-4.5}$
10–25	$\sim E^{-3.9}$	$\sim E^{-5.3}$	$\sim E^{-6.0}$	$\sim E^{-5.4}$
25–50	$\sim E^{-5}$	$\sim E^{-6.1}$	$\sim E^{-6.7}$	$\sim E^{-5.9}$
	$E_1 \leqslant E_2$ (10 eV)			
5–10	$\sim E_1^{-1.6}$	$\sim E_1^{-1.3}$	$\sim E_1^{-1.8}$	$\sim E_1^{-1.6}$
	$E_1 \geqslant E_2$ (10 eV)			
10–25	$\sim E_1^{-1.5}$	$\sim E_1^{-1.7}$	$\sim E_1^{-2.1}$	$\sim E_1^{-1.9}$
25–50	$\sim E_1^{-1.5}$	$\sim E_1^{-1.8}$	$\sim E_1^{-2.3}$	$\sim E_1^{-1.9}$

As is revealed from the table, the low-energy partial TCS (e.g., $E_1=E_2\sim 5-10$ eV) falls off very slowly as compared to the intermediate and high energies and the slope of the $1s$ TCS (see also Fig. 7) is much less than that of the others ($2s$, $2p$ and $1s+2s+2p$). Another important feature should be noted from this table that for $E_1\neq E_2$, the power of the exponent decreases as compared to the $E_1=E_2$ case throughout the energy range. This again indicates the better efficiency of the $\bar{H}$ production for unequal energies ($E_1\neq E_2$) of the active and the passive e^+'s over a wider energy ranges (E_1).

IV. CONCLUSIONS

The salient features of the present study are as follows. At very low incident energies the present TBR cross section for the $\bar{H}$ formation in the $2p$ state is found to be the dominant process among the three states $1s$, $2s$, $2p$ while at intermediate and high incident energies, the ground state ($1s$) cross section dominates for both equal and unequal energies of the two positrons with some exceptions for the latter case ($E_1>E_2$).

Substantially higher cross sections are noted in the TBR model than in the other RR or charge transfer processes leading to antihydrogen in the present energy range. The partial TCS is found to be significantly higher when the active e^+ energy is greater than that of the spectator e^+ (i.e., $E_1>E_2$) than for $E_1=E_2$ or for $E_1<E_2$.

For a more efficient production of $\bar{H}$ for a wider energy range, the unequal ($E_1>E_2$) distribution of energy between the active and the spectator positrons could be suggested rather than the equal one ($E_1=E_2$). The present $\bar{H}$ formation cross section decreases with increasing e^+ energy (i.e., temperature) but does not follow any simple scaling law in the present energy range ($\sim 5-10$ eV) corroborating (qualitatively) the existing experiments at extreme low energies ($\sim 10^{-4}$ eV). However, both the partial and the sum TCS obey different power laws for different incident energy ranges.

The present model is not supposed to be suitable for the experimental extreme low energy regime and a more sophisticated theory is needed. The limitations of the present model (described in the Introduction) particularly with respect to an external magnetic field might have some effects on the present results and may be considered in a future work. Finally, the present TBR results might give some physical insights to the future detailed $\bar{H}$ experiments.

[1] Andre Gsponer and Jean-Pierr Hurni, e-print arXiv:physics/0507125v2.
[2] R. L. Forward, J. Br. Interplanet. Soc. **35**, 387 (1982).
[3] G. Gabrielse, S. L. Rolston, L. Haarsma, and W. Kells, Phys. Lett. A **129**, 38 (1988).
[4] G. Gabrielse, Adv. At., Mol., Opt. Phys. **50**, 155 (2005).
[5] M. H. Holzscheiter and M. Charlton, Rep. Prog. Phys. **62**, 1 (1999).
[6] S. M. Li, Z. J. Chen, Q. Q. Wang, and Z. F. Zhou, Eur. Phys. J. D **7**, 39 (1999).
[7] Shu-Min Li, Yan-Gang Miao, Zi-Fang Zhou, Ji Chen, and Yao-Yang Liu, Phys. Rev. A **58**, 2615 (1998).
[8] Saverio Bivona, Riccardo Burlon, Gaetano Ferrante, and Claudio Leone, Opt. Express **14**, 3715 (2006).
[9] J. W. Humberston, M. Charlton, F. M. Jacobsen, and B. I. Deutch, J. Phys. B **20**, L25 (1987).
[10] J. W. Darewych, J. Phys. B **20**, 5917 (1987).
[11] S. N. Nahar and J. M. Wadehra, Phys. Rev. A **37**, 4118 (1988).
[12] M. Charlton, Phys. Lett. A **143**, 143 (1990).
[13] S. Tripathi, C. Sinha and N. C. Sil, Phys. Rev. A **42**, 1785 (1990).
[14] J. Mitroy and A. T. Stelbovics, Phys. Rev. Lett. **72**, 3495 (1994).
[15] J. Mitroy and G. Ryzhikh, J. Phys. B **30**, L371 (1997).
[16] S. Tripathi, R. Biswas, and C. Sinha, Phys. Rev. A **51**, 3584 (1995).
[17] J. Mitroy, Phys. Rev. A **52**, 2859 (1995).
[18] J. Mitroy and A. T. Stelbovics, J. Phys. B **27**, L79 (1994).
[19] D. B. Cassidy, J. P. Merrison, M. Charlton, J. Mitroy, and G. Ryzhikh, J. Phys. B **32**, 1923 (1999).
[20] A. Chattopadhyay and C. Sinha, Phys. Rev. A **74**, 022501 (2006).
[21] M. Amoretti *et al.*, Nature (London) **419**, 456 (2002).
[22] M. Amoretti *et al.*, Phys. Rev. Lett. **91**, 055001 (2003).
[23] M. Amoretti *et al.*, Phys. Lett. B **578**, 23 (2004).
[24] M. Amoretti *et al.*, Phys. Lett. B **583**, 59 (2004).
[25] N. Madsen *et al.*, Phys. Rev. Lett. **94**, 033403 (2005).
[26] M. Amoretti *et al.*, Phys. Rev. Lett. **97**, 213401 (2006).
[27] G. Gabrielse *et al.*, Phys. Rev. Lett. **89**, 213401 (2002).
[28] G. Gabrielse *et al.*, Phys. Rev. Lett. **89**, 233401 (2002).
[29] G. Gabrielse *et al.*, Phys. Lett. B **548**, 140 (2002).
[30] G. Gabrielse *et al.*, Phys. Rev. Lett. **93**, 073401 (2004).
[31] G. Gabrielse *et al.*, Phys. Rev. Lett. **98**, 113002 (2007).
[32] G. Gabrielse *et al.*, Phys. Lett. B **507**, 1 (2001).
[33] A. Speck, C. H. Storry, E. A. Hessels, and G. Gabrielse, Phys. Lett. B **597**, 257 (2004).
[34] T. Pohl, H. R. Sadeghpour, and G. Gabrielse, Phys. Rev. Lett. **97**, 143401 (2006).
[35] G. Andresen *et al.*, Phys. Rev. Lett. **98**, 023402 (2007).
[36] A Torii Hiroyuki *et al.* (private communication).
[37] F. Robicheaux, J. Phys. B **40**, 271 (2007).
[38] M. E. Glinsky and T. M. O'Neil, Phys. Fluids B **3**, 1279 (1991).
[39] Leonard I. Schiff, *Quantum Mechanics*, 3rd ed., Physics Series (McGraw-Hill International Editions, Singapore, 1968), p. 113.
[40] F. Robicheaux, Phys. Rev. A **70**, 022510 (2004).
[41] F. Robicheaux, Phys. Rev. A **73**, 033401 (2006).
[42] I. S. Gradshteyn and I. M. Ryzhik, *Tables and Integrals Series and Products* (Academic, New York, 1980), p. 933.
[43] A. Messiah, *Quantum Mechanics* (North-Holland, Amsterdam, 1966), Vol. 1, p. 481.
[44] R. Biswas and C. Sinha, Phys. Rev. A **50**, 354 (1994).
[45] B. Nath and C. Sinha, Eur. Phys. J. D **6**, 295 (1999).
[46] B. Nath and C. Sinha, J. Phys. B **33**, 5525 (2000).
[47] D. Ghosh and C. Sinha, Phys. Rev. A **69**, 052717 (2004).